18th Brazilian Congress of Thermal Sciences and Engineering
November 16-20, 2020 (Online)

ENC-2020-0310
NUMERICAL SIMULATION ASSESSMENT FOR PREDICTING FLOW THROUGH SUPERSONIC SEPARATOR NOZZLE

Igor Longhi Baxmann
Reinaldo Marcondes Orselli, Phd
Univesidade Federal do ABC, centro de engenharia, modelagem e ciências sociais aplicadas, Avenida dos Estados, 5001, Santo André, SP, Brazil
igorlbaxmann@gmail.com
reiorselli@gmail.com
Ricardo Galdino da Silva, Phd
Instituto de Aeronáutica e Espaço, departamento de ciência aeroespacial e tecnologia, Praça Marechal Eduardo Gomes, 50, São José dos Campos, SP, Brazil
ri_galdino@yahoo.com
Bruno do Carmo Souza, Phd
Universidade de São Paulo, Escola Poltécnica, departamento de engenharia mecânica, São Paulo, SP, Brazil.
bruno.carmo@usp.br

Abstract. *The purpose of this study is to investigate numerically the physical characteristics of flows through* supersonic *nozzles used for supersonic gas separators. Numerical simulations of a convergent-divergent nozzle are carried out whose geometry is based on experimental results available in the literature. Different turbulence models are applied, and the numerical simulations result obtained by them are compared with their corresponding experimental results. The aim of present work is to assess the capability of CFD based on RANS turbulence modeling to predict the flow behavior within the supersonic nozzle, including particular features such as pressure variation along the nozzle, shock wave position and its topology due to interaction with the boundary layer.*

Keywords: *Computational fluid Dynamics, Turbulence models, Mechanics of fluids, shock wave, Supersonic Separator*

1. INTRODUCTION

The growth in the exploration of fossil fuels in offshore regions after the discovery of the pre-salt increased the demand for technological solutions that would facilitate the commercialization of oil and its derivatives directly in the extraction regions (Lima, 2016).

With regard to natural gas, the most notable challenges are related to the removal of impurities that are extracted with it. Fossil fuel can present water particles, the presence of acids and high concentrations of CO2, making the displacement for decontamination in onshore regions dangerous and expensive, since the combination of acids with hydrocarbons results in corrosive compounds. Thus, it is necessary to implement techniques and equipment that allow the purification of natural gas directly at the extraction point or in nearby locations. A possible technology for this application is the supersonic gas separator, since it has a low energy cost, it is compact and has no moving parts (Liu, 2014; Arinelli, 2015).

The mechanism consists of a Laval nozzle with divergent and convergent sections where the gases are accelerated to supersonic speed and expanded generating a drop in temperature. With cooling, some of the contaminants such as CO2 are condensed while the fossil fuel remains in the gaseous state. By imposing rotating flow forces the heavier condensed components are pushed towards the wall where collectors are carefully placed to remove them, as shown in Figure 1.

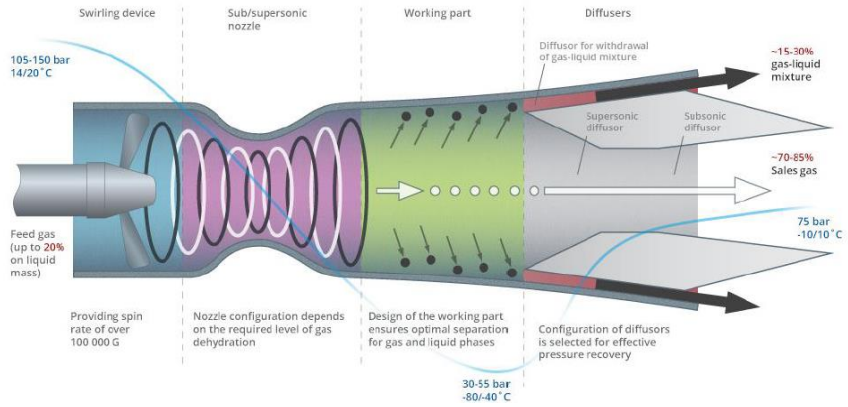

Figure 1: Different parts of 3S Supersonic Separator by ENGO Engineering. Adapted from (Imaev et al., 2014).

The internal flow of the supersonic separators presents complex physical behaviors like the formation of shock waves and consequent interactions with the boundary layer. The increase in entropy and temperature characteristic of shock waves, directly impact the functioning of the equipment, and therefore studies must be carried out for the design and optimization of such devices.

Nevertheless, the quality and accuracy of the numerical simulations to predict the behavior of such gases in supersonic separators are paramount to perform a proper design and optimization of the system. One of the typical issues related to numerical simulation of highly turbulent flows stands on the capacity of the CFD based on turbulence modeling to predict the flow behavior, in the case here applied for supersonic separators.

2. OBJECTIVE

The purpose of this work is to carry out numerical simulations to assess the capacity of the numerical methodology to predict the flow behavior inside a supersonic convergent-divergent nozzle with reference to experimental results available as the one available in the work of Papamoschou (2008). In particular, the case corresponds to a convergent-divergent supersonic nozzle geometry used in the work of Papamoschou (2008) with a pressure ratio (NPR) range between 1.3 and 1.5, which corresponds to a typical pressure ratio for the operation of supersonic gas separators as, for example, shown in Fig. 1. In the present work, the commercial code ANSYS FLUENT is used for the numerical simulations whose solver is based on the Finite Volume method.

In order to carry out the numerical simulations, the flow computational domain is considered firstly as two-dimensional, followed by a preliminary study with the flow domain as three-dimensional. Due to the high turbulent flow, different turbulence models are used. As such, some turbulence models implemented in ANSYS FLUENT are considered and assessed with reference to the corresponding experimental data presented in Papamoschou (2008), in particular, the cases are available with NPR of 1.31 and 1.42. Not only the pressure variation data along the nozzle is compared but also some flow features such as location of the shock wave, its topology, interaction with the boundary layer and flow separation. The turbulence models considered for this work are the following: Spalart-Allmaras (Spalart & Almaras,1992), k-ε Standard (Lauder & Spalding, 1974), k-ε RNG (Yakhot et al , 1992), k-ω Standard (Wilcox, 1998) and k-ω SST (Menter, 1994), all models implemented in Ansys Fluent (see Ansys Inc, 2013).

3. METHODOLOGY

In the commercial code ANSYS FLUENT, the governing flow equations of Navier-Stokes are resolved numerically. The flow domain is discretized by applying the finite volume method (Versteeg & Malalaskera, 2007). There are two main numerical solvers in the ANSYS FLUENT code, one is known as Density-Based solver and the other is the Pressure-Based solver. For the density-based solver, all discretized linearized system of equations is solved in one single matrix, as all state flow variables are solved in a coupled manner. For the pressure-based solver, the linear system of the discretized equations is resolved in a segregated or sequential manner. For the results presented here, the segregated solver is considered with the state equation incorporated to deal with the high compressible nature of the flow inside the nozzle (see methodology in Maliska, 2004). The advantage of the segregated solver with respect to the density-based solver is that it requires less computer memory and it has a lower computational cost per interaction.

In order to deal with the high turbulent flow, and avoid the prohibitive computational cost of resolving all flow turbulent scales, the Navier-Stokes equations are time-averaged with each flow variable decomposed with a time-averaged and a fluctuating part (known as Reynolds decomposition). As a result of the time-averaged Navier-Stokes equations, a non-linear term dependent on the fluctuating part of the flow velocities remains, which is known as Reynolds-stress tensor. In order to close the set of equations of the averaged Navier-Stokes equations, also known as

RANS (Reynolds Averaged Navier-Stokes) equations, additional transport equations are need due to Reynolds-stress tensor term as it is dependent on the fluctuating part of the flow velocities. Firstly, the Reynolds-stress tensor term can be related to the mean flow by considering the Boussinesq hypothesis (see Versteeg & Malalaskera, 2007), which in turn introduces a new coefficinet known as turbulent viscosity due to its physical interpretation related to the additional turbulent flow mixing with respect to the fluid viscosity. Following that, the unknown turbulent viscosity is modeled by relating it with new turbulent flow variables. Finally, to close the RANS equations, additional transport equations for these turbulent flow variables are proposed. There are several turbulence models in the literature that propose a relation for the turbulent viscosity with different turbulent flow variables and transport equations (Versteeg & Malalaskera, 2007). The turbulent models considered for this work are the following: Spalart-Allmaras (Spalart,1992), k-ε Standard (Lauder Spalding, 1974), k-ε RNG (Yakhot et al , 1992), k-ω Standard (Wilcox, 1988) and k-ω SST (Menter, 1992); all models are available in Ansys Fluent code (details in Ansys Inc, 2013).

4. RESULTS

4.1 Geometry and mesh

The nozzle geometry used from the experimental work of Papamoschou (2008) is presented in Fig. 2. It can be noted a deflection mechanism that enables variation of the sectional area ratio (outlet section area divided by throat area), in the present study an area ratio of 1.4 was considered. The geometry used for the numerical simulations was actually adapted from the design shown in Fig. 2 due to the fact that some details of the nozzle geometry were not provided. The convergent geometry was made by adjusting a quadratic polynomial from the nozzle geometry of Arina (2004). At the divergent part of the nozzle geometry, the trumpet shape design as mentioned in Papamoschou (2008) was adjusted with an arc of radius 149.67 cm. The completed geometry is illustrated in Fig 3 with a total throat height of 2.286 cm (or 1.143 if only half is used for the computational domain), corresponding to an area ratio of 1.4. Due to the symmetric nature of the flow through the convergent-divergent nozzle, the geometry of Papamoschou (2008) was made as symmetrical, and so the computational domain was made with only the upper half of the nozzle as showed in Figure 3.

For the nozzle with a two-dimensional domain as shown in Fig. 3, a structured mesh was built with 770 cells along the streamwise direction of the nozzle and 50 cells along its height with a total of 38500 cell volumes. The y+, non-dimensional wall distance, set for this mesh configuration was close to 2 in the shock region and 12 in regions further away.

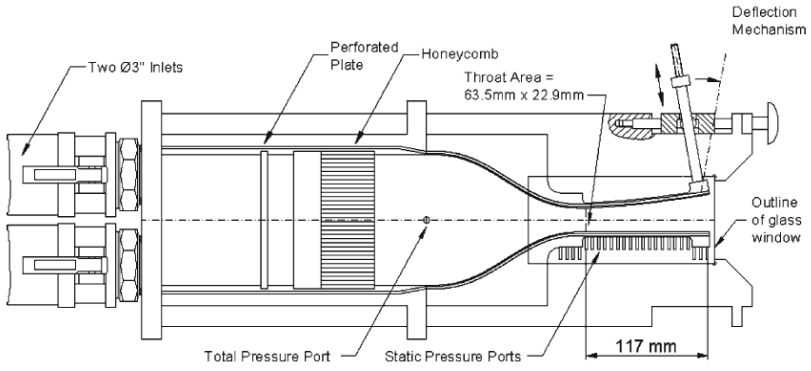

Figure 2: Papamoschou (2008)'s original geometry.

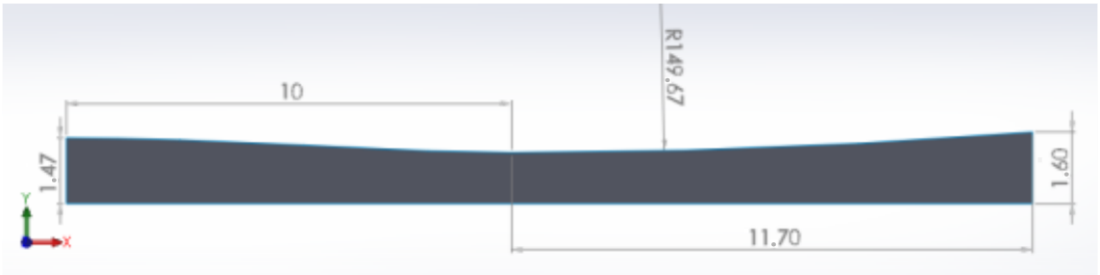

Figure 3: Upper half of the nozzle. Dimensional in centimeters (cm).

4.2 Numerical setup

Based on the typical nozzle pressure ratio (NPR) of supersonic separators as shown in Fig. 1 in the range between 1.3 and 1.5, and considering the experimental data available of Papamoschou (2008), two pressure ratios were defined for this work, respectively NPR=1.33 and NPR=1.42. As the results with NPR=1.33 and NPR=1.42 were quite similar, including their discrepancies with respect to the corresponding experimental data of Papamoschou (2008), the results are shown only for the case with NPR=1.42. For the boundary conditions of the numerical simulations, total pressure and total temperature at the inlet section (reservoir condition) were set, and static pressure and total temperature fixed at the outlet section. Adiabatic no-slip wall was applied at the upper boundary of nozzle and symmetry condition for the axis line. The fluid is considered as an ideal gas calorically perfect and the values used for the boundary conditions are presented in Table 1.

Table 1: Boundary Conditions (a) NPR=1.33 (b) NPR=1.42

(a)	**Static Pressure**	**Total Pressure**	**Total temperature**
Inlet	129488 Pa	134762.3 Pa	291.39 K
Outlet	100000 Pa	-	291.39 K

(b)	**Static Pressure**	**Total pressure**	**Total temperature**
Inlet	138248 Pa	143881.5 Pa	291.39 K
Outlet	100000 Pa	-	291.39 K

For the two-dimensional simulations, according to the segregated pressure-based solver in Ansys Fluent, in order to deal with the pressure-velocity coupling, it was used a scheme known as Couple (Ansys Inc, 2013). This algorithm allows to solve the momentum and continuity equation together, which may bring a better numerical convergence with respect to other well-known schemes such as SIMPLE. Besides that, for all simulations a second order upwind scheme was applied for all convective terms of the transport equations (Barth and Jespersen, 1989), and the diffusive terms were discretized by a central differencing scheme (Versteeg & Malalasekera, 2007). In order to obtain the pressure on the faces of the control volume, an interpolation scheme based on a ‘staggered’ control volume arrangement was employed for all cases (known in ANSYS Fluent as PRESTO, PREssure Staggering Option, Ansys Inc, 2013).

With regard to numerical convergence criteria according to Ansys Inc (2013), as a general reference, at least maximum residual value of 1e-3 for all transport equations, and a maximum residual value of 1e-6 for the energy transport equation, is recommended. Residuals are defined in Ansys Fluent as the imbalance of each discretized transport equation summed over all cells of the domain at the current iteration scaled by the flux of the main variable at the cell center according to each equation (Ansys Inc, 2013).. Table 2 shows the residual values obtained for each turbulence model all with the same mesh. In particular, for the k-ω SST, it was not possible to get lower residual values below the recommendation according to Ansys Fluent. In general for this problem of a supersonic nozzle, it has been shown to be difficult to make the residuals to get lower values for all turbulence models tested, in particular with the k-ω SST, a possible explanation is due the outlet boundary that is quite close to the shock wave position in association with the boundary layer interaction with the shock wave followed by flow separation, as such a complex flow with high flow gradients.

Table 2: Residuals for two-dimensional study. Nut is the variable of turbulence used for the additional one transport equation of the SA (Spalart-Almaras) model.

models	Continuity	x-velocity	y-velocity	energy	k	**ε**	**ω** / Nut
k-ε RNG	9.7176e-07	2.1111e-09	1.7910e-10	5.6770e-10	6.4561e-09	1.6303e-08	-
k-ε STD	3.4749e-04	1.3192e-06	4.7286e-07	4.7928e-07	1.2428e-04	2.6742e-04	-
k-ω SST	7.6212e-06	3.8416e-08	4.7319e-09	4.1699e-08	2.1539e-06	-	4.2269e-06
k-ω STD	2.4970e-03	1.8483e-05	2.8816e-06	4.7191e-06	2.7285e-04	-	3.2193e-04
SA	9.9256e-11	1.6312e-13	2.0503e-14	9.2326e-14	-	-	2.2907e-13

4.3 Two-dimensinal results

To verify the influence of the mesh resolution in the results, two simulations with different mesh refinements were considered: a standard mesh with 38500 cell volumes, used for all 2D simulations, and a more refined mesh with twice more, totalizing 77000 cell volumes. The curves of the static pressure along the nozzle obtained by both cases with standard and refined mesh were compared as shown in Fig. 4. As observed in Fig. 4, both cases did not show significant difference of the static pressure values if compared with each other and the experimental data, as such the standard mesh case with 35800 volumes is sufficiently refined, and used for all 2D simulations.

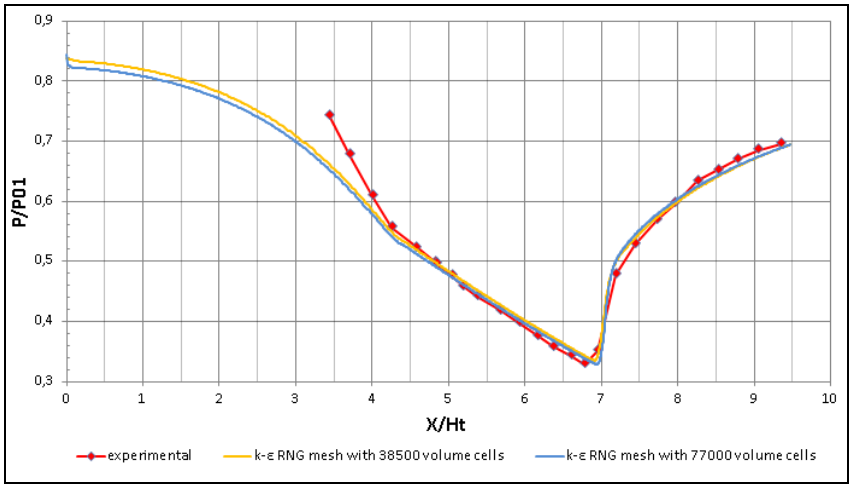

Figure 4: Curve of the ratio of static pressure (P/P01) against the nozzle length (X/Ht, with Ht the nozzle height at the throat) for NPR=1.42 and area ratio of 1.4. k-ε RNG model with standard mesh of 38500 volume cells and refined mesh with 77000 volume cells. The experimental data is from Papamoschou (2008). P01 is total pressure at the nozzle intet.

For the standard mesh, the nondimensional wall distance of the first cell adjacent to the wall known as y plus (definition in Versteeg & Malalasekera. 2007) presented a range of values from 1 to 20 along the nozzle. Thus, in order to resolve the flow gradients on the wall region, and dealing with the broad range of y plus values, a blended wall model is used known as 'enhanced wall treatment' in ANSYS Fluent, it is based on a two layer model with a blend damping function to make a smooth transition between a near wall model for the viscous sublayer region typically with y plus below 5 to a full logarithm law of the wall for regions typically with y plus above 30 (Ansys Inc, 2013).

In Figure 5, the curves of the pressure ratio, with respect to the inlet total pressure P01, along the nozzle axis line is presented for each turbulence model considered, and are compared with the corresponding experimental data measured by Papamoschou (2008). Observing the pressure ratio curves of Fig. 5, the best agreement with the corresponding experimental curve was obtained with the k-ε RNG turbulence model, followed closely by the Spalart-Allmaras and k-ω SST models. The same behavior was obtained with the case of NPR=1.33 (not shown).

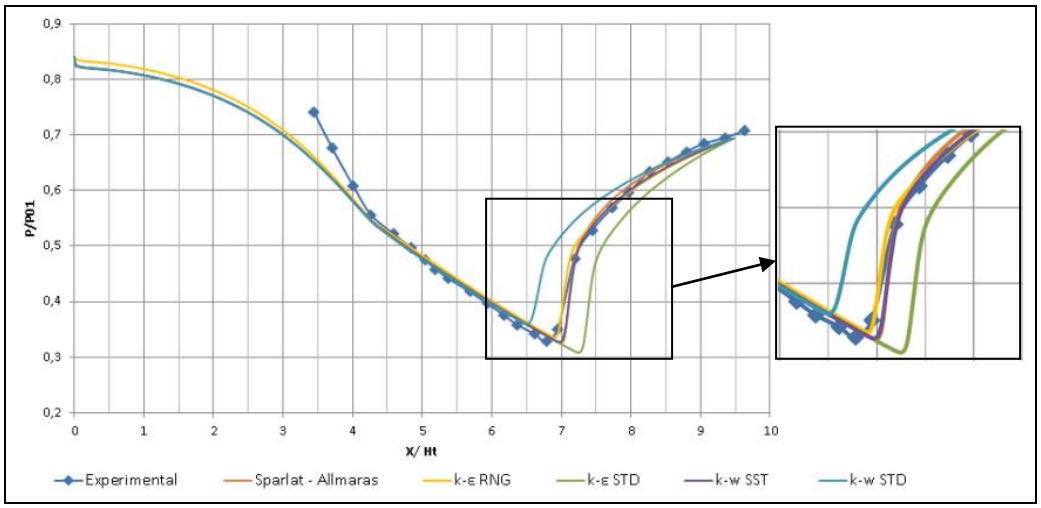

Figure 5: Curve of the ratio of static pressure (P/P01) against the nozzle length (X/Ht, with Ht the nozzle height at the throat) for NPR=1.42 and area ratio of 1.4 for the 2D simulations. Left side is a zoom of the curves around the shock wave position. The experimental data is from Papamoschou (2008). P01 is total pressure at the nozzle intet.

For this nozzle geometry corresponding to an area ratio of 1.4 and NPR in the range between 1.3 and 1.5, the shock wave is normal occurring inside the nozzle between the throat and the outlet section. For NPR=1.42, a Schlieren photography of the shock wave is illustrated in Fig. 6c, the shock wave presents a lambda shape topology towards the wall due to its interaction with the boundary layer. In addition, observing Fig. 6c, it should be noted that following the shock wave, flow separation occurs due to the strong adverse pressure caused by the sudden increase of pressure through the shock wave itself.

In Figure 6a and 6b, the static pressure fields obtained, respectively, with the k-ε RNG and k-ω SST models are shown, and it can be compared with the Schlieren photography of Papamoschou (2008), Fig. 6c. The shape and position of the shock wave obtained by the numerical simulations with both turbulence models (Fig. 6a and 6b) are quite similar, if compared with the Schlieren photography, by both predicting the lambda shape topology.

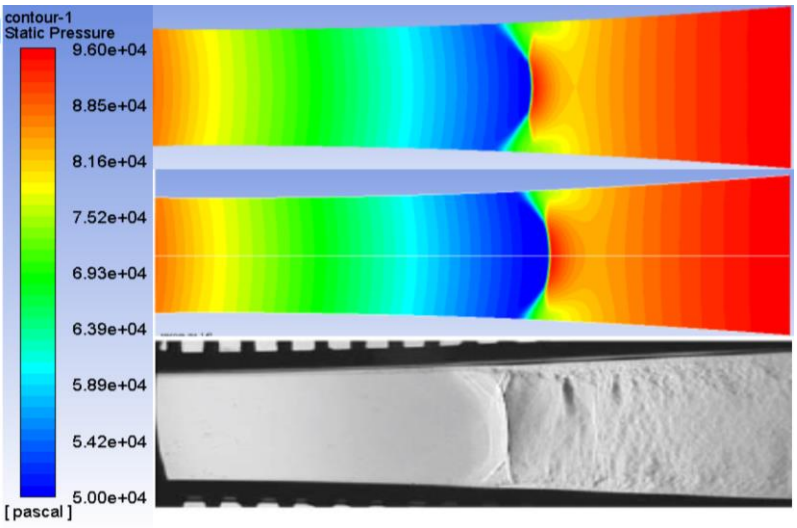

Figure 6: Static pressure NPR 1.42 (a) k-ε RNG (b) k-ω SST (c) Schlieren photography from Papamoschou (2008). NPR = 1.42. Area ratio = 1.4.

4.4 Tri-dimensional results

For the three-dimensional nozzle flow domain, a structured mesh was built with 350 cells along the streamwise direction of the nozzle, 45 cells along its height and the geometry was extended in the spanwise direction with a distance of 63.5mm (2.78 times the throat height), and discretized with 70 cell volumes. Due to the symmetric nature of the flow, only a quarter of the nozzle section area was considered for the simulation, as such symmetry boundary conditions at one lateral (left side) and bottom faces, as shown in Fig. 3, were imposed. At the upper and right lateral faces, a no-slip adiabatic wall was applied. As shown in Fig. 7, towards the walls the mesh was refined to capture the high flow gradients within the boundary layer. Finally, the 3D mesh built for the flow domain (quarter of nozzle section area) reached a total of 1055250 cell volumes and the range of the nondimensional wall distance of the first cell volume, Y plus, was between 2 and 40 for this configuration.

In view of the limited computational resources, it was considered NPR=1.42 in all simulations, and the turbulence models used were restricted to the k-ε RNG and k-ω SST. For the convective terms of the discretized transport equations, an upwind second-order spatial differencing method was applied (Barth and Jespersen, 1989) and the diffusive terms were discretized by a central differencing scheme. In order to deal with the pressure–velocity coupling due to the segregated solver algorithm, the pressure-based scheme PISO was employed, and the PRESTO algorithm was employed to obtain the pressure on the faces of the control volumes (Versteeg and Malalasekera, 2007).

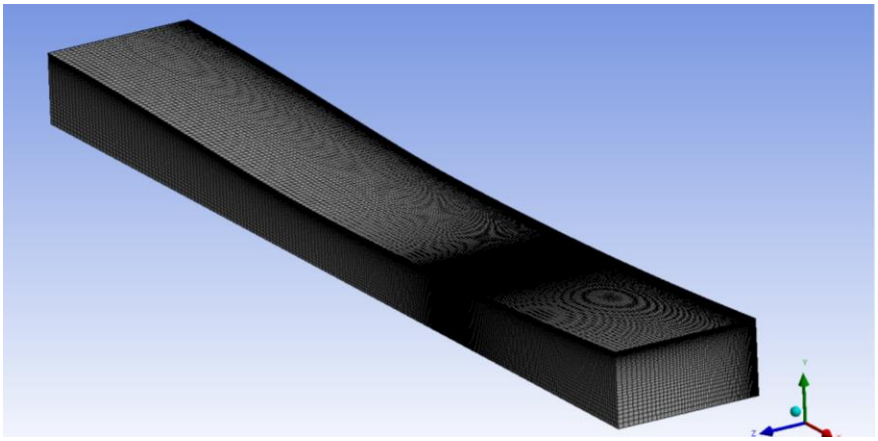

Figure 7: Tridimensional Mesh with 1055250 cell volumes, domain with a quarter of nozzle section total area.

Table 3: Residuals for the 3D simulations.

Model	Continuity	x-velocity	y-velocity	z-velocity	energy	k	ω or ε
k-ω SST	8.7617e-04	1.6411e-04	2.7217e-06	3.4280e-06	2.5331e-06	5.3960e-04	2.5567e-04
k-ε RNG	2.4020e-03	5.8396e-05	5.1136e-06	3.9474e-06	2.4780e-06	2.3638e-04	6.5821e-04

In order to verify the numerical convergence, the residual values (as defined in section 4.2) for each discretized transport equation for both simulations are presented in Table 3. As a general guide for numerical convergence, according to Ansys fluent (2013), it is reccommended to check if at least the maximum residual values are below 1e-3 for all transport equations and less than 1e-6 for the energy equation. In particular for the continuity equation, the residual value is above 1e-3 for the k-ε RNG and more than 1e-6 for both models for the energy equation. In fact, along the running process of each simulation, difficulties have been found to get a lower residual. As aforementioned in section 4.2, the fact that the outlet boundary is quite close to the shock wave position in combination with the interaction of the shock wave and the boundary layer with flow separation, and the typical 3D recirculating flow at the wall corners bring more complexity to the simulation, including the inherent high flow gradients, as such reaching numerical convergence for this problem has been found to be quite challenging.

In Fig. 8, the static pressure curves along the 3D nozzle obtained by the k-ε RNG and k-ω SST are shown and compared with the corresponding experimental data of Papamoschou (2008). The results show that the curve predicted by the k-ε RNG represent well the experimental curve all long the shock wave up to the nozzle outlet. In spite of that a slight difference of the shock position is observed approximately of X/Ht = 0.25 (Ht is the nozzle throat height). In contrast, the results of the static pressure curve obtained by the k-ω SST model do not reproduce the corresponding experimental curve behavior, even not representing the presence of the typical sharp normal shock wave. Additional verifications and investigation are in progress to identify possible issues or setting up inconsistencies, including the effect of mesh refinement, which may possibly improve the results of with k-ω SST model, particularly with respect to better predicting the sharp normal shock wave behavior

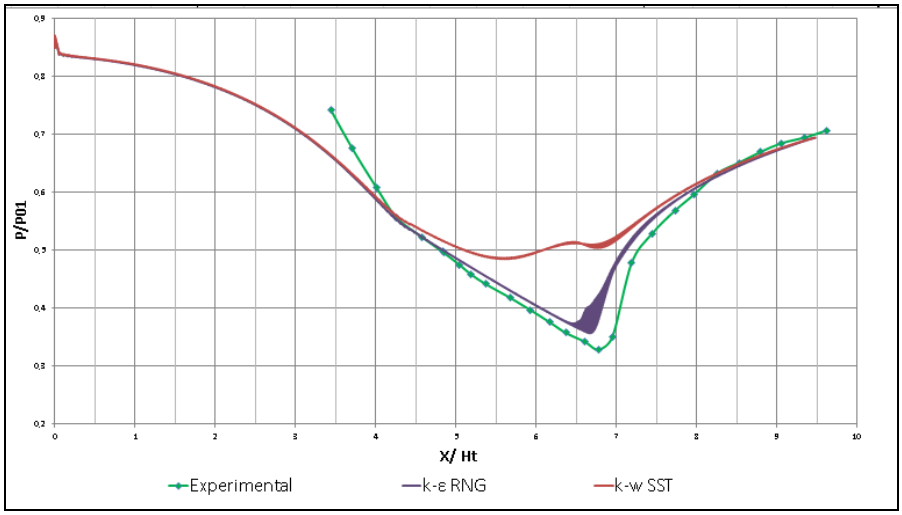

Figure 8: Curve of the ratio of static pressure (P/P01) against the nozzle length (X/Ht, with Ht the nozzle height at the throat) for NPR=1.42 and area ratio of 1.4 for the 3D simulations with k-ε RNG and k-ω SST models. The static pressure numerical data were obtained from the lateral wall plane of the nozzle, which explains a range of values for each X position. The experimental data is from Papamoschou (2008). P01 is total pressure at the nozzle inlet.

Moreover, by comparing the static pressure curves of the k-ε RNG with the 3D and 2D simulations as shown in Fig. 9, it is noted that the 3D results presented a shock wave position to occur more upstream with respect to the results predicted by 2D case. The more upstrem position of shock wave obtained by the 3D simulation can be explained by the additional energy losses between the outlet and the shock wave, which pushes the shock wave position to occur further from the outlet if compared with the 2D corresponding simulation. In fact, the presence of the wall boundary layer along the upper and lateral walls as well as the 3D flow separation downstrem the shock wave, and the recirculating (or secondary) flow at the wall corners are the main features that brings an increase of the energy losses for the 3D case with respect to the 2D simulation. In spite of the additional energy losses for the 3D, the pressure curves predicted by 3D simulations are still following well the pressure variation behavior obtained experimentally.

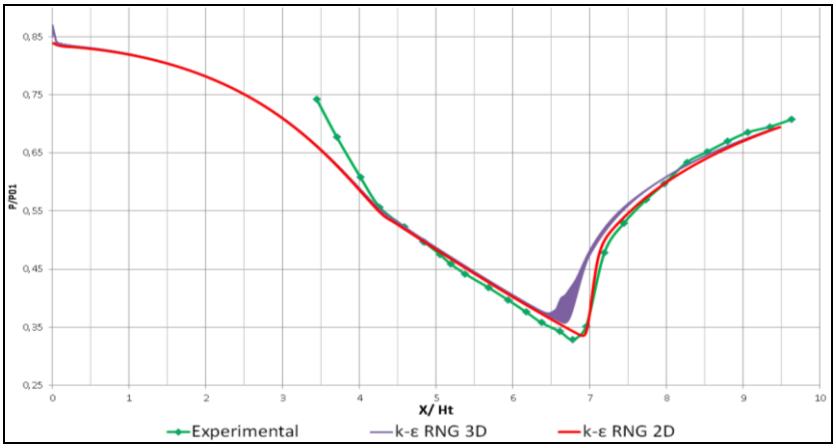

Figure 9: Curve of the ratio of static pressure (P/P01) against the nozzle length (X/Ht, with Ht the nozzle height at the throat) for NPR=1.42 and area ratio of 1.4, comparing 2D and 3D k-ε RNG results. The experimental data is from Papamoschou (2008). P01 is total pressure at the nozzle inlet.

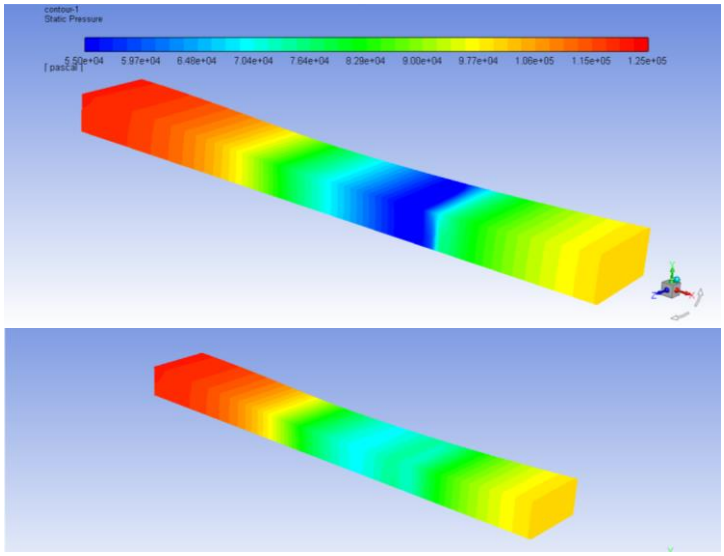

(a)

(b)

Figure 10: Static pressure contour: (a) k-ε RNG, (b) k-ω SST.

In Figure 10, the contours of static pressure obtained by each turbulence model are shown, which allows to have a broader qualitative view of the pressure variation all along the nozzle. As shown with the pressure curves in Fig. 8, for the k-ω SST the region where the shock wave should occur the pressure gradients **is** much smoother and more diluted if compared with the corresponding k-ε RNG case. In addition, Fig. 11 also allows a broad view of the flow behavior with the Mach number field along the nozzle for the two turbulence models. As visualized in Fig. 9 with the k-ω SST, despite being supersonic downstream the throat, the Mach number variation is much more diluted if compared with the k-ε RNG case, as such the supersonic flow acceleration along the nozzle up the shock wave is not well represented by the k-ω SST case for the 3D simulation.

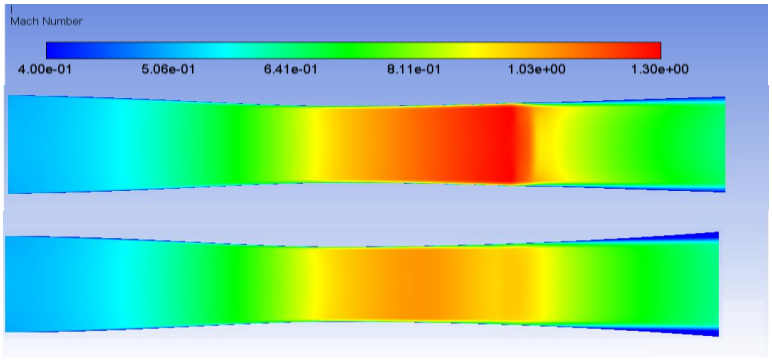

(a)

(b)

Figure 11: Mach number countours: (a) k-ε RNG; (b) k-ω SST.

Due to conservation of energy of the flow across the shock wave, the total temperature does not change across the shock wave, considering ideal gas calorically perfect within flow regions not affected significantly by the flow viscosity, as such the total temperature field is presented in Fig. 12. Thus, observing Fig. 10, even that the numerical simulations have not fully converged, according to the residual criteria, as shown in Table 3, the conservation of energy represented by the total temperature across the shock wave, despite the presence of high flow gradients, has been maintained. In addition, due the flow separation downstream the shock wave, energy losses occur along the nozzle wall, as such the total temperature varies accordingly as clearly observed in Fig. 12.

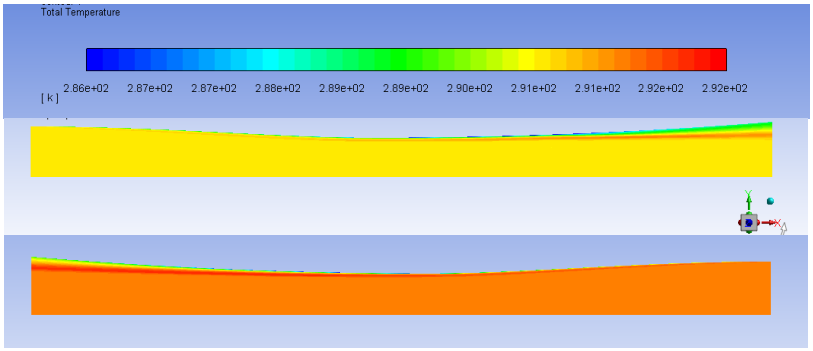

Figure 12: Total temperature contours: (a) k-ε RNG (a); (b) k-ω SST.

The vorticity magnitude field at the nozzle outlet section is presented in Fig. 13. Observing both fields, it can be noted high vorticity near the corner between the upper and lateral walls, which indicates the presence of a local recirculation. In fact, the occurrence of recirculation or secondary flow is typical at the wall corners for flows through rectangular nozzle section as shown, for example**,** in Wilcox (1998). By comparing k-ω SST and k-ε RNG fields in Fig. 13, it is noted that the vorticity magnitude size and strength obtained by both models are quite different, however there are no experimental data available to assess how accurate is the predictions of the simulations. In particular, Wilcox (1998) highligheted the difficulty of the turbulence models to well predict these recirculations around the wall corners, especially with turbulence models based on the Boussinesq hypothesis, suggesting also the use of nonlinear turbulence models to better predict such recirculating flows.

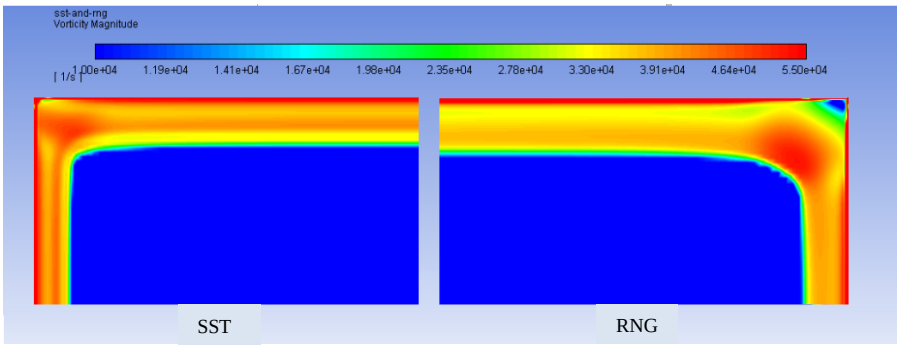

Figure 13: Vorticity magnitude field at the nozzle outlet for k-ω SST (left) and k-ε RNG (right).

5. CONCLUSION

In general, the k-ε RNG was the model that presented the static pressure curves with the best agreement among the turbulence models tested when compared with the corresponding experimetal curves given by Papamoshou (2008). For the 3D results, there has been found difficulty to get convergence due the obtained high numerical residuals in particular with the k-ω SST and the 3D simulations. In general, the k-ε RNG was able to predict the main behavior of the flow through the supersonic nozzle, in particular with respect to capturing the presence of a sharp normal shock in accordance with the corresponding experimental data of Papamoshou (2008).

In order to carry on the present work for the 3D case, investigations of the solver, turbulence model parameters, and mesh refinement are in progress to get numerical convergence (lower numerical residuals) as well as improving the results with the k-ω SST model. Finally, additional turbulence models could be tested for the 3D simulations, such as the SA (Spallart-Almaras), and more sofistaced models such as the Reynolds Stress model (RSM) and non-linear k-ε models as suggested, for example, in Wilcox (1998) to well predict the secondary flow at the wall corners.

6. ACKNOWLEDGEMENTS

We gratefully acknowledge support of the RCGI – Research Centre for Gas Innovation, hosted by the University of São Paulo (USP) and sponsored by FAPESP – São Paulo Research Foundation (2014/50279-4) and Shell Brasil, and the strategic importance of the support given by ANP (Brazil's National Oil, Natural Gas and Biofuels Agency) through the R&D levy regulation.

7. REFERENCES

Ansys Inc (2013), "FLUENT USER'S GUIDE".< https://www.ansys.com/>.

Arinelli L.O., Medeiros J.L., Araújo O.Q., 2015. "Performance analysis and comparison of membrane permeation versus supersonic separator for CO2". Removal from a plausible natural gas of Libra field, Brazil, Offshore technology conference, OTC-26164-MS, Rio de Janeiro-RJ, 27-29.

Arina R., 2004. "Numerical simulation of near-critical fluids". *Applied Numerical Mathematics*, 51: 409-426.

Barth, T.J., Jespersen, D.C., 1989. The design and application of upwind schemes on unstructured meshes, AIAA PAPER 89-0366.

Hirsh C., 2007. *Numerical Computation of Internal and External Flows*. Vol I, 2nd edition, Elsevier.

Hirsh C., 1990. *Numerical Computation of Internal and External Flows*. Vol II, 1st edition, John Willey & sons Ltd.

Imaev S.Z., Bagirov L.A., Borisov V.E., Voytenkov E.V., 2014. "New low temperature process of CO2 recovery from natural gases", SPE 171427, *SPE Asia Pacific Oil & Gas Conference and Exhibition*, Adelaide, Australia.

Launder B.E., Spalding D.B., 1974. "The numerical computation of turbulent flows". *Computer Methods in Applied Mechanics and Engineering*, 3 (2), 269-289.

Lima, P. C. R. 2016 "Gás Natural: a sua utilização na geração de energia elétrica no Brasil". jan. 2020. < http:// www.desenvolvimentistas.com.br/blog/blog/2016/01/14/a-solucao-para-o-co2-do-pre-sal/>.

Liu, X. "Investigation on Separation Efficiency in Supersonic Separator with Gas-Droplet Flow Based on DPM Approach. *Separation Science and Technology* (Philadelphia), Taylor & Francis, v. 49, n. 17, p. 2603–2612,

Maliska C., 2004. *Transferência de calor e mecânica dos fluidos computacional*. 2nd edition, LTC (in portuguese).

Menter F.R., 1994. "Two-Equation Eddy-Viscosity Turbulence Models for Engineering Applications". *AIAA Journal, 32 (8),* 1598-1605.

Papamoschou D., Zill A., Johnson A., 2008 . "Supersonic flow separation in planar nozzles". *Springer-Verlag*.

Spalart P.R and Allmaras S.R.,1992. "A One-Equation Turbulence Model for Aerodynamic Flows*", AIAA Paper 92-0439*.

Vesteeg, H. K. and Malalasekera,W., 2007. *An introduction to computational fluid dynamics - the finite volume method*. [S.l.]: Addison-Wesley-Longman, 2007.

Wilcox D.C., 1998. *Turbulence Modeling for CFD*. 2nd Ed., DCW Industries.

Yakhot V., Orszag S.A., Thangam S., Gatski T.B. & Speziale C.G. 1992. *Development of turbulence models for shear flows by a double expansion technique*, Physics of Fluids A, Vol. 4, No. 7, pp1510-1520.